Plasma Exosomal miRNAs Associated With Metabolism as Early Predictor of Gestational Diabetes Mellitus

Zhixin Ye,[1] Songzi Wang,[2] Xiaoqing Huang,[1] Peisong Chen,[2] Langhui Deng,[2] Shiqi Li,[1] Suiwen Lin,[1] Zilian Wang,[1] and Bin Liu[1]

Diabetes 2022;71:2272–2283 | https://doi.org/10.2337/db21-0909

To date, the miRNA expression profile of plasma exosomes in women whose pregnancy is complicated by gestational diabetes mellitus (GDM) has not been fully clarified. In this study, differentially expressed miRNAs in plasma exosomes were identified by high-throughput small-RNA sequencing in 12 pregnant women with GDM and 12 with normal glucose tolerance (NGT) and validated in 102 pregnant women with GDM and 101 with NGT. A total of 22 exosomal miRNAs were found, five of which were verified by real-time qPCR. Exosomal miR-423–5p was upregulated, whereas miR-122–5p, miR-148a-3p, miR-192–5p, and miR-99a-5p were downregulated in women whose pregnancy was complicated by GDM. IGF1R and GYS1 as target genes of miR-423–5p, and G6PC3 and FDFT1 as target genes of miR-122–5p were associated with insulin and AMPK signaling pathways and may participate in the regulation of metabolism in GDM. The five exosomal miRNAs had an area under the curve of 0.82 (95%CI, 0.73, ∼0.91) in early prediction of GDM. Our study demonstrates that dysregulated exosomal miRNAs in plasma from pregnant women with GDM might influence the insulin and AMPK signaling pathways and could contribute to the early prediction of GDM.

Gestational diabetes mellitus (GDM) is one of the most common disorders during pregnancy (1); it increases the risk of numerous perinatal complications, including preeclampsia, macrosomia, and neonatal hypoglycemia. Moreover, GDM is associated with later development of obesity, type 2 diabetes, and increased cardiovascular risk for mother and offspring (2).

Generally, GDM is diagnosed during gestational weeks (gws) 24–28 by oral glucose tolerance test (OGTT) (3), but evidence shows that hyperglycemia exists before 24–28 gws and is associated with adverse maternal, fetal, and neonatal outcomes (4). Clinical guidelines call for early screening of GDM (5–7), and new biomarkers are needed to improve prediction efficacy (8). Of note, high levels of fatty acid–binding protein 4 (9), visfatin (10), and asprosin (11) were proposed as potential biomarkers of GDM. In a cohort of 474 pregnant women, angiopoietin-like protein 8 improved the prediction of GDM as early as 12–16 gws (12). Recently, authors of a nested case–control study reported that seven urinary metabolites could predict GDM, with an area under the curve (AUC) of 0.993 at around 12 gws (13).

Insulin resistance is the most important pathogenetic factor in development of GDM, and it normally develops earlier than hyperglycemia does (2). The AMPK signaling pathway also plays a critical role in regulating lipid and glucose metabolism (14). Thus, the determination of biomarkers related to metabolism may provide important considerations for early prediction of GDM.

Exosomes are extracellular vesicles generated by various cells and contain many components, including DNAs, RNAs, and proteins. Exosomes play critical roles in mediating intercellular communication and have great potential for use in disease diagnosis and therapies (15, 16). Exosomes regulate the development and progression of diseases, including cancers (17), neurodegenerative disease (18), and metabolic complications (19). The cargo carried by exosomes contributes to altered crosstalk among skeletal muscle, liver, adipose tissue, and pancreas during the development of diabetes and obesity (20–22). In addition, exosomes are also associated with the pathogenesis of preterm birth (23) and preeclampsia (24). In GDM, Salomon

[1]Department of Obstetrics and Gynecology, the First Affiliated Hospital of Sun Yat-sen University, Guangzhou, People's Republic of China
[2]Department of Laboratory Medicine, the First Affiliated Hospital of Sun Yat-sen University, Guangzhou, People's Republic of China
Corresponding author: Bin Liu, liubn@mail.sysu.edu.cn

Received 11 October 2021 and accepted 2 August 2022

This article contains supplementary material online at https://doi.org/10.2337/figshare.20421585.

et al. (25) first found that the concentration of exosomes in plasma was increased in women whose pregnancy is complicated with GDM. Gillet et al. (26) reported elevated miR-520h levels in extracellular vesicles in pregnancies with GDM. Kandzija et al. (27) found increased dipeptidyl peptidase IV levels in placental extracellular vesicles from GDM cases. These studies showed a tight association between GDM and exosomes; however, the mechanism by which exosomes and their contents regulate metabolic signaling pathways has not been fully clarified. Moreover, the application of exosomal constituents in early screening of GDM requires further elucidation.

The purpose of this study was to profile circulating exosomal miRNAs, investigate their regulatory roles in GDM, and inspect differentially expressed miRNAs as early biomarkers of GDM.

RESEARCH DESIGN AND METHODS

Patients and Samples

Women aged 18–45 years with singleton pregnancies were invited to participate in this study. The exclusion criteria for this study were individuals with preexisting diabetes. Written informed consent was obtained from all participants. This study was approved by the ethics committee of the First Affiliated Hospital of Sun Yat-sen University in Guangzhou, China.

The research cohort contained three sets: *1*) the discovery set, consisting of 12 pregnant women with GDM and 12 with normal glucose tolerance (NGT) for small-RNA next-generation sequencing (NGS); *2*) the validation set with 102 pregnant women with GDM and 101 with NGT for verification of dysregulated miRNAs; and *3*) the prediction set with 30 pregnant women with GDM and 60 with NGT from a nested case–control study based on a prospective cohort started at 10–16 gws. The diagnosis of GDM was according to International Association of Diabetes and Pregnancy Study Groups 2015 guidelines (28). Fasting blood samples were collected (BD Vacutainer PLUS Tubes; EDTA) and prepared for plasma.

Exosome Isolation

Exosomes were isolated from plasma using differential ultracentrifugation and the ExoQuick kit (System Biosciences, EXOQ5TM-1). For ultracentrifugation, samples were centrifuged at 2,000*g* for 30 min and 12,000*g* for 45 min. The supernatant fluid was passed through a 0.22 μm sterile filter (Steritop; Millipore, Billerica, MA) and then centrifuged at 110,000*g* for 120 min (Optima XE-100, SW41 Ti Rotor; Beckman). The pellet was resuspended in 200 μL of PBS (pH 7.4). We used 500 μL of plasma for exosome precipitation, according to the manufacturer's instructions.

Transmission Electron Microscopy

For transmission electron microscopy analysis, a 10 μL aliquot of fresh exosomes isolated by ultracentrifugation was added to a 400-mesh formvar/carbon-coated copper grid for 1 min and then negatively stained with 2% uranyl acetate for 30 s under dark conditions. Then a JEM-1400 electron microscope (JEOL Ltd.) was used to assess the morphology of the exosomes.

Nanoparticle Tracking Analysis

Nanoparticle tracking analysis was applied to analyze the distribution of diameters and concentration of exosomes isolated by ultracentrifugation, using a NanoSight NS300 (Malvern Instruments).

Western Blot Analysis

Exosome specific biomarkers, including CD9 (Cell Signaling Technology no. 13174; Research Resource Identifier [RRID] AB_2798139), CD63 (Proteintech no. 25682–1-AP; RRID AB_2783831), and TSG101 (Abcam no. ab125011; RRID: AB_10974262), were determined through Western blotting. Lysis buffer was used to break down cells for the radioimmunoprecipitation assay. Exosomes isolated by the ExoQuick kit were lysed in radioimmunoprecipitation assay lysis buffer containing the protease inhibitor phenylmethylsulfonyl fluoride. Protein contents were determined using a bicinchoninic acid assay protein assay kit (CW0014S; CWBIO). We separated 20 μg of lysate and transferred it to polyvinylidene fluoride membranes, then incubated the lysate with primary antibodies and appropriate horseradish peroxidase–conjugated secondary antibodies.

Cell Culture

Male human hepatoma cells (HepG2), female normal human hepatic cells (LO2), and female human embryonic kidneys (293T) were obtained from the American Type Culture Collection and cultured in a high-glucose (4.5 g/L) DMEM solution supplemented with 10% FBS.

Internalization of Exosomes by HepG2 Cells

HepG2 cells ($n = 1 \times 10^5$) were seeded in a 15 mm culture dish and incubated with exosomes dyed with the red fluorescent linker PKH26 (MINI26–1KT; Sigma-Aldrich) for 8 h at 37°C. The cells were washed twice with PBS, and then fixed with 4% formaldehyde for 10 min and stained with Hoechst 33342 (C1025; Beyotime) and F-actin (AMJ-KT0003; Amyjet). The samples were analyzed using a laser scanning confocal microscope (LSM780; Zeiss).

Glucose-Uptake Assay

HepG2 cells were seeded in 48-well plates at 1×10^5 cells/well with or without intervention for 48 h at 37°C. After being starved in glucose-free medium for 3 h, the cells were incubated with 40 μM 2-[*N*-(7-nitrobenz-2-oxa-1,3-diazol-4-yl) amino]-2-deoxy-D-glucose (2-NBDG) (Apexbio; B6035) for 30 min. The 2-NBDG fluorescence intensity was analyzed by flow cytometry at 488 nm (excitation) and 530 nm (emission).

Small-RNA NGS

The purity of RNA was assessed using an ND-1000 Nanodrop; each RNA sample had an A260:A280 ratio >1.8 and A260:A230 ratio >2.0. RNA integrity was evaluated using the Agilent 2200 TapeStation and each sample had the RNA Integrity Number equivalent >7.0. Next, the RNA samples were subjected to library preparation using the NEBNext Multiplex Small RNA Library Prep Set for Illumina (Illumina) and sequenced on the HiSeq2500 (read length, 1 × 50 bp). The small RNA NGS data were submitted to the National Center for Biotechnology Information Gene Expression Omnibus (accession number GSE192813).

Analysis of Sequencing Data

The miRDeep2 program was used to identify known miRNAs from FASTQ files. The human genome sequence (GRCh38) obtained from the Ensembl database was used to build a bowtie index. The remaining reads were aligned to miRBase v21 miRNA sequences (www.mirbase.org). Differential expression of miRNAs was analyzed using DESeq2 (version 3.10) with fold change ≥1.5 or ≤0.67, and $P \leq 0.05$ as the threshold.

RNA Extraction and Real-Time qPCR

The miRNeasy Mini Kit (no. 217004, QIAGEN) was used to purify miRNA from exosomes isolated by ExoQuick kit. *Caenorhabditis elegans* cel-miR-39–3p (5′−UCACCGGGUGUAAAUCAGCUUG−3′; Ribobio, Guangzhou, China) was taken as an exogenous miRNA spiked-in control of plasma exosomal miRNAs. In cell experiments, U6 was used to normalize miRNAs extracted from cells. Total RNAs were extracted from cells using Trizol (Invitrogen). Real-time qPCR was performed using TB Green TM Premix Ex Taq TM II (Tli RNaseH plus) (no. RR820A, TaKaRa) on a LightCycler System (Roche) in triplicate. Primer sequences are provided in Supplementary Table 1. The mean of the NGT group was used as the reference and relative expression levels (GDM vs. NGT) were calculated using the comparative cycle threshold method.

Bioinformatic Analyses

TargetScan 7.2, Tarbase 8.0, and miRDB were used to predict potential targets of miRNAs. The enrichment analysis of gene ontology and associated pathways was performed in R (version 3.6) with the *clusterProfiler* package. Statistics were corrected for multiple testing using the Benjamini–Hochberg procedure.

Lentivirus-Mediated Overexpression of miRNAs and Transcriptome NGS

miRNA expression vectors containing an miRNA precursor overexpression cassette or a scrambled sequence for control were produced by GeneChem. The resulting viruses were then used to infect HepG2 cells. Then RNAs were extracted, reverse-transcribed to cDNA, and sequenced on an Illumina Novaseq 6000 (LC-Bio Technology) with 150-bp paired-end sequencing.

miRNA Transfection

miRNA mimics, inhibitors, and negative controls (RiboBio) were transfected into cells using a Lipofectamine 3000 transfection reagent (ThermoFisher Scientific) for 48 h. miRNA mimics were transfected at a concentration of 50 nmol/L, whereas miRNA inhibitors were transfected at a concentration of 100 nmol/L.

Plasmid Construction and Luciferase Reporter Assay

The target gene prediction for miRNAs was conducted with TargetScan Human 7.2 (https://www.targetscan.org/vert_72/) (29). The wild-type or mutant 3′ untranslated region (3′UTR) of targets was cloned into pmirGLO Dual-Luciferase miRNA target expression vector using *Nhel* and *Xbal* restriction endonuclease sites. The luciferase reporter constructs were cotransfected with miRNA mimic or negative controls into 293T cells in 96-well plates. Luciferase activity was measured 48 h posttransfection with a dual-luciferase reporter assay system (Promega, GLoMax) and normalized to *Renilla* activity.

Statistical Analysis

The data obtained from this study were analyzed using R (version 3.6.0). Continuous variables were presented as mean ± SD. To compare the differences between two groups, an unpaired Student *t* test was performed only if the data were normally distributed. If the data were not normally distributed, a Wilcoxon rank-sum test was used. For binary variables, a χ^2 test was used to compare the differences between two groups. To examine the relationships between clinical parameters and miRNAs, a Spearman correlation test was used. Binomial logistic regression was used to identify associations between miRNAs and pregnancy outcomes. Receiver operating characteristic (ROC) curve analysis was conducted to assess the predictive power of differentially expressed miRNAs based on a logistical regression model. Net reclassification improvement (NRI) was calculated using the R package *nricens* to evaluate the improvement of predictive accuracy in predicting GDM when miRNAs were combined into the conventional model. Statistical significance was defined as $P < 0.05$.

Data and Resource Availability

The data generated and/or analyzed during this study are available from the corresponding author upon reasonable request.

RESULTS

Clinical Characteristics of the Research Cohort

The clinical characteristics of the participants are listed in Table 1. No statistically significant differences were found in maternal age, gravity, or parity between the GDM and NGT groups. In the discovery and validation sets, women with GDM had a higher mean weight and BMI before and during pregnancy compared with the NGT group.

Table 1—Baseline characteristics of participants

	Discovery set*			Validation set†			Predictive set‡		
	NGT (n = 12)	GDM (n = 12)	P	NGT (n = 101)	GDM (n = 102)	P	NGT (n = 60)	GDM (n = 30)	P
Age, years	34.17 ± 4.15	34.25 ± 3.17	0.956	33.50 ± 3.47	33.53 ± 4.16	0.964	32.68 ± 3.86	33.63 ± 3.81	0.272
Gestational age, weeks									
At enrollment	13.94 ± 1.81	14.70 ± 2.44	0.403	14.60 ± 2.90	14.92 ± 3.72	0.529	14.44 ± 1.88	14.33 ± 1.27	0.790
At OGTT	25.35 ± 1.87	26.11 ± 2.15	0.365	25.55 ± 1.22	25.49 ± 1.73	0.794	26.37 ± 1.23	26.63 ± 1.49	0.405
At delivery	39.08 ± 1.17	38.76 ± 0.81	0.441	38.97 ± 1.31	38.26 ± 1.16	<0.001	39.23 ± 0.92	38.87 ± 1.19	0.130
Weight, kg									
Pregravid	51.25 ± 4.86	58.54 ± 5.93	0.003	52.80 ± 6.94	56.25 ± 8.05	0.002	54.80 ± 7.66	55.17 ± 7.39	0.831
At enrollment	52.74 ± 5.55	61.00 ± 6.27	0.002	53.79 ± 6.72	56.84 ± 8.11	0.014	56.39 ± 8.06	56.73 ± 7.52	0.851
At OGTT	59.22 ± 5.35	66.48 ± 6.95	0.009	59.31 ± 6.78	62.13 ± 8.27	0.023	63.08 ± 7.58	62.75 ± 7.68	0.852
At delivery	64.78 ± 6.47	70.29 ± 6.69	0.052	66.04 ± 6.94	66.18 ± 8.14	0.901	68.77 ± 7.95	65.73 ± 9.21	0.121
BMI, kg/m^2									
Pregravid	20.32 ± 1.82	22.86 ± 2.32	0.007	21.26 ± 4.79	22.41 ± 3.25	0.060	21.10 ± 2.55	21.83 ± 2.29	0.205
At enrollment	20.93 ± 2.33	23.81 ± 2.34	0.006	20.98 ± 2.48	22.66 ± 3.29	0.001	21.66 ± 2.74	22.45 ± 2.34	0.199
At OGTT	23.48 ± 2.06	25.93 ± 2.40	0.014	23.14 ± 2.44	24.64 ± 3.18	0.001	24.22 ± 2.37	24.83 ± 2.28	0.271
At delivery	25.67 ± 2.37	27.41 ± 2.32	0.083	25.75 ± 2.38	26.23 ± 3.13	0.239	26.50 ± 2.44	25.97 ± 2.80	0.382
OGTT glucose value, mmol/L									
Fasting	4.07 ± 0.42	4.97 ± 0.40	<0.001	4.24 ± 0.24	4.68 ± 0.45	<0.001	4.25 ± 0.24	4.63 ± 0.47	<0.001
1 h	6.90 ± 1.59	11.30 ± 1.22	<0.001	6.88 ± 1.26	10.86 ± 1.08	<0.001	6.90 ± 1.19	9.89 ± 1.64	<0.001
2 h	6.46 ± 1.03	9.37 ± 1.27	<0.001	6.01 ± 0.92	9.39 ± 1.16	<0.001	6.07 ± 0.99	9.05 ± 1.31	<0.001
HbA_{1c}, %	4.59 ± 0.33	5.22 ± 0.25	<0.001	4.57 ± 0.25	5.08 ± 0.37	<0.001	4.57 ± 0.23	5.11 ± 0.27	<0.001
HbA_{1c}, mmol/mol	26.83 ± 3.56	33.50 ± 2.88	<0.001	26.50 ± 2.80	32.00 ± 4.07	<0.001	26.52 ± 2.56	32.23 ± 2.98	<0.001
Multiparous (%)	7 (58.3)	9 (75.0)	0.665	52 (55.9)	53 (59.6)	0.729	20 (37.7)	11 (37.9)	0.999
Cesarean section (%)	9 (75.0)	8 (66.7)	0.913	46 (49.5)	59 (66.3)	0.032	19 (35.8)	13 (44.8)	0.575
Neonatal sex									
Male (%)	6 (50.0)	8 (66.7)	0.679	55 (59.1)	47 (53.4)	0.531	31 (58.5)	12 (41.4)	0.211
Female (%)	6 (50.0)	4 (33.3)		38 (40.9)	41 (46.6)		22 (41.5)	17 (58.6)	

Data reported as mean ± SD, unless otherwise indicated. *Participants included at 24–28 gws for finding differentially expressed miRNAs in exosome through small-RNA sequencing. †Participants included at 24–28 gws for validating differentially expressed miRNAs in exosome. ‡Participants included at 10–16 gws for verifying early predictive power of exosomal miRNAs.

Plasma Exosomes of GDM and NGT Pregnancy

Transmission electron microscopy showed that exosomes were approximately 100 nm in diameter and had a characteristic morphology with a central depression attributed to cellulose embedding and encapsuled by a limiting membrane (Fig. 1*A*). Vesicles were positive for CD63, Tsg101, and CD9 (Fig. 1*B*). The difference of mean exosome diameter between the GDM and NGT groups was not statistically significant (122 ± 7 nm vs. 117 ± 16 nm; P = 0.56, n = 5/group), but a secondary peak at around 60 nm was observed in the distribution curve of the NGT group, indicating that smaller exosomes might exist in the plasma of some pregnant women (Fig. 1*C*). In exosome concentrations, no statistically significant differences were found between the GDM and NGT groups ($5.30 \times 10^{10} \pm 6.20 \times 10^{10}$ vs. $7.37 \times 10^{10} \pm 8.59 \times 10^{10}$ particles/mL plasma; P = 0.71).

Internalization of Exosomes From Pregnant Women With GDM and Those With NGT

To investigate the effects of exosomes on cellular glucose metabolism, HepG2 cells were incubated with PKH26-dyed exosomes isolated from plasma of women with GDM and those with NGT. Using confocal microscopy, we visualized the internalization of PKH26-dyed exosomes into HepG2 cells within 8 h of coincubation (Fig. 1*D*). Notably, exosomes from women with GDM women reduced cellular glucose uptake by ∼59% as compared with those from women with NGT (Fig. 1*E*).

Exosomal miRNA Expression Profile and Validation of Differentially Expressed miRNAs

Small-RNA NGS was performed to reveal the differences in exosomal contents between the GDM and NGT groups (n = 12). In the GDM group, 36 miRNAs were upregulated and 67 were downregulated (Fig. 2*A*). Of the exosomal miRNAs detected with basemean >1,000, five miRNAs were upregulated and 17 miRNAs were downregulated in the GDM group (Fig. 2*B*).

The 22 dysregulated exosomal miRNAs were further verified in the validation set, where five miRNAs were confirmed as differentially expressed miRNAs. Among them, miR-423–5p was upregulated, whereas miR-122–5p, miR-148a-3p, miR-192–5p, and miR-99a-5p were downregulated

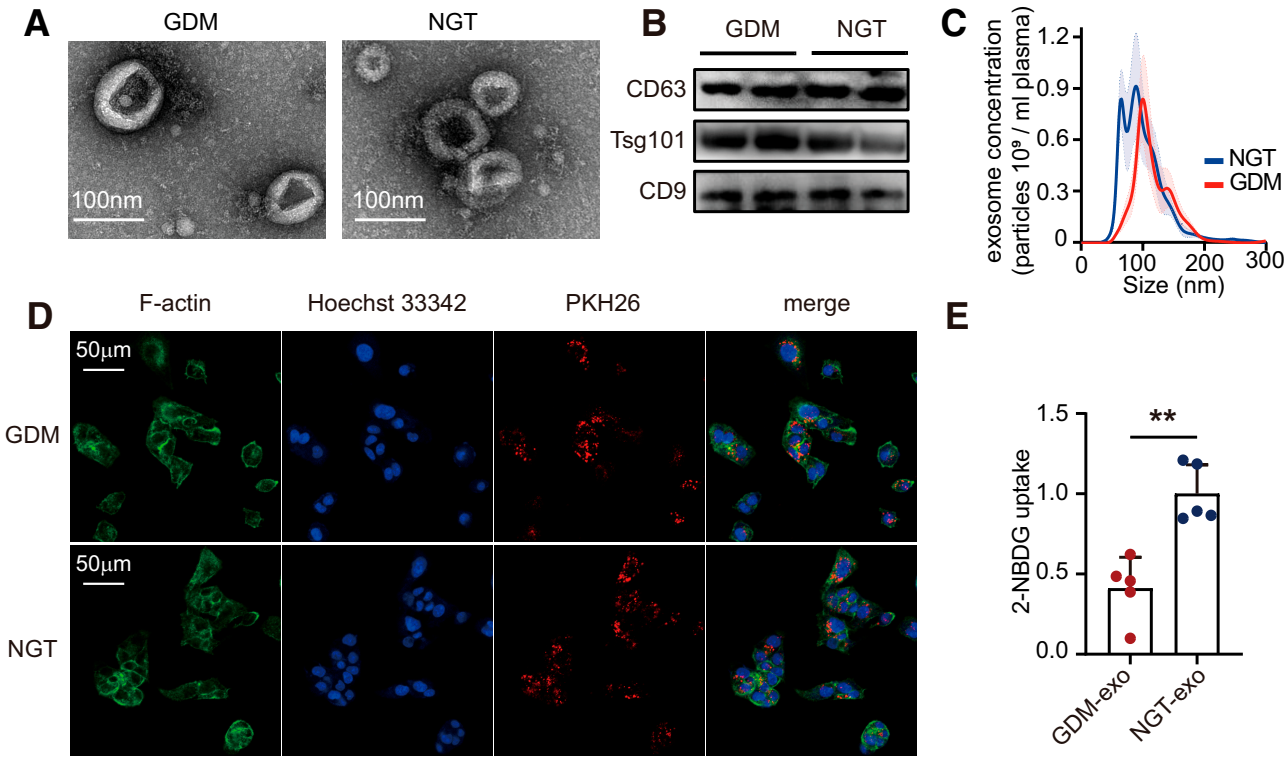

Figure 1—Characteristics of plasma exosomes from pregnant women with GDM and pregnant women with NGT. (*A*) Representative TEM images of plasma exosomes from pregnant women with GDM and those with NGT. Exosomes in both groups were disc-like in morphology, with a central depression. Scale bar, 100 nm. (*B*) The expression of exosome-specific markers CD63, Tsg101, and CD9 assessed by Western blotting was not significantly different between GDM and NGT groups. (*C*) The distribution of exosome diameters detected by NanoSight NS300. (*D*) PKH26-dyed exosome internalization into HepG2 cells under confocal microscopy. Green, cytoskeleton stained by F-actin dye; blue, nucleus stained by Hoechst 33342; red, exosomes stained by PKH26 dye. (*E*) Exosomes from pregnant women with GDM reduced cellular glucose uptake compared with exosomes from pregnant women with NGT. Exo, exosome. $^{**}P < 0.01$.

in the GDM group (Fig. 2*C*). The remaining 17 miRNAs did not show any significant differences between groups (Supplementary Fig. 1).

Associations Between Exosomal miRNAs and Clinical Features

The associations between expression of exosomal miRNAs and related clinical features were analyzed in the validation set (Table 2). Exosomal miR-423–5p was positively correlated with fasting plasma glucose (FPG) level (r = 0.18; P = 0.01), and miR-122–5p and miR-148a-3p were negatively correlated with prepregnancy BMI, BMI at OGTT, 1-h plasma glucose level (1h-PG), 2h-PG, and HbA_{1c}. miR-192–5p was negatively associated with prepregnancy BMI, FPG, 1h-PG, 2h-PG, and HbA_{1c}. Inverse correlations of exosomal miR-99a-5p with BMI at OGTT, 1h-PG, 2h-PG, and HbA_{1c} existed. When analyzed separately in each group, miR-148a-3p and miR-192–5p remain negatively correlated with 2h-PG in the NGT group, and the other correlations mostly followed the same trends of the whole group but without statistically significance (Supplementary Table 2). These results indicate that change in expression levels of plasma exosomal miRNAs could be used to distinguish the GDM group from the NGT group but did not have enough power to reflect the intragroup differences in plasma glucose levels.

Early Prediction of GDM by Plasma Exosomal miRNAs

To investigate the predictive value of exosomal miRNAs on GDM, we tested the expression of the five differentially expressed miRNAs in nested case–controlled groups with 30 women with GDM and 60 women with NGT at 10–16 gws. Exosomal miR-122–5p, miR-148a-3p, miR-192–5p, and miR-99a-5p in plasma were downregulated in the GDM group (Fig. 3*B–E*, left), but no statistically significant difference was found for miR-423–5p (Fig. 3*A*, left). After adjusting for age, BMI at enrollment, ALT, and AST, miR-122–5p (adjusted odds ratio [OR] 0.33; 95% CI 0.14–0.79), miR-148a-3p (adjusted OR 0.10; 95% CI 0.02–0.41), miR-192–5p (adjusted OR 0.10; 95% CI 0.02–0.40), and miR-99a-5p (adjusted OR 0.02; 95% CI 0.002–0.19) were inversely associated with the risk of GDM (Supplementary Table 3).

In ROC curve analysis, the five miRNAs showed the potential to predict GDM (Fig. 3*A–E*, right). The AUC of the five miRNAs combined for early prediction of GDM was 0.82 (95% CI 0.73–0.91). This result was superior to the base model, which combined FPG, maternal age, and

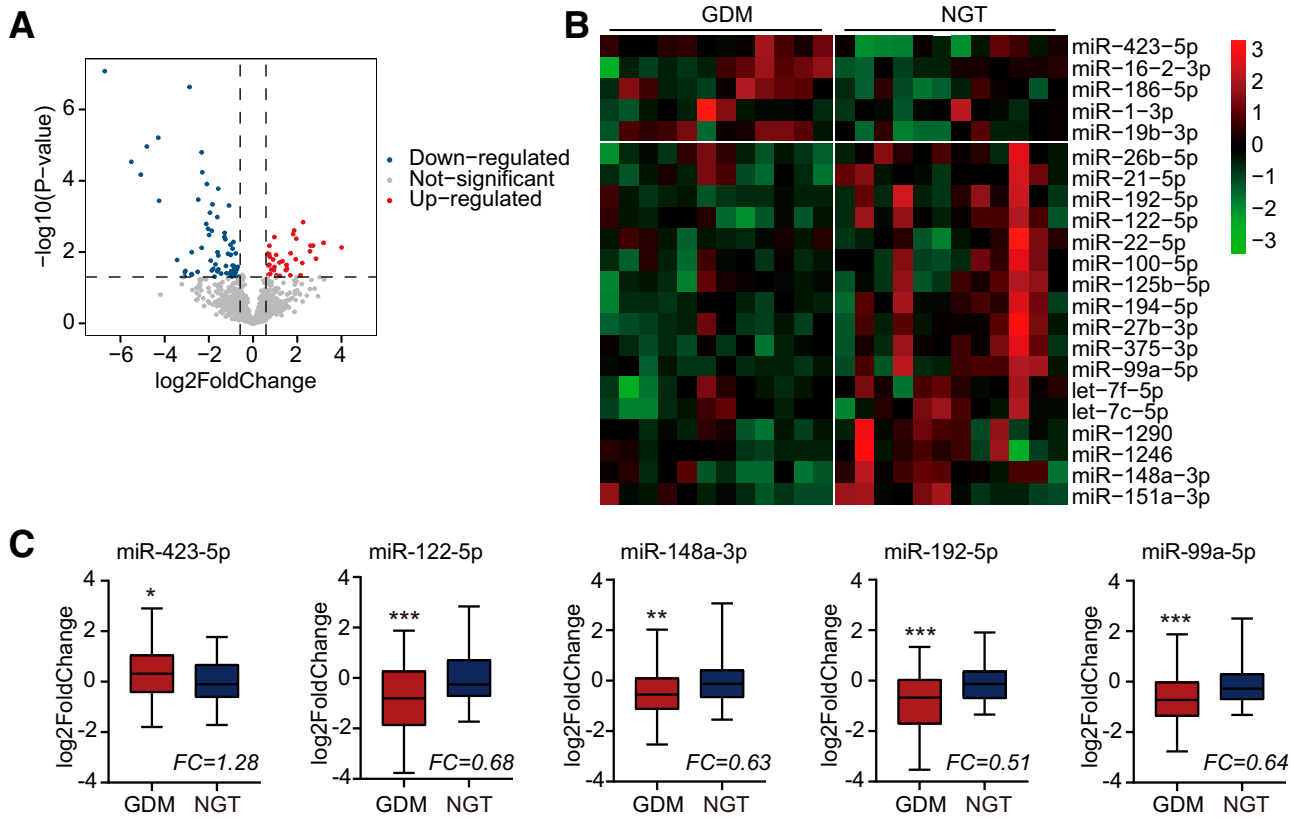

Figure 2—Exhibition of dysregulated exosomal miRNAs. (*A*) Volcano plot showing 36 upregulated and 67 downregulated miRNAs. (*B*) Heat map displaying the 22 differentially expressed exosomal miRNAs with basemean >1,000. (*C*) Validated miRNA expression in plasma exosomes derived from pregnant women with GDM (n = 102) and NGT (n = 101). Cel-miR-39-3p was used as an internal control. Data are shown as log2 fold change compared with the NGT group. *$P < 0.05$, **$P < 0.01$, ***$P < 0.001$. FC, fold change.

Table 2—Spearman correlation analysis investigating the association between exosomal miRNAs and clinical indicators

	miR-423–5p		miR-122–5p		miR-148a-3p		miR-192–5p		miR-99a-5p	
	r	*P*	*r*	*P*	*r*	*P*	*r*	*P*	*r*	*P*
Age	0.00	0.99	0.09	0.19	−0.04	0.56	−0.03	0.66	0.04	0.62
Prepregnancy BMI	0.03	0.68	−0.20	0.01	−0.17	0.02	−0.17	0.02	−0.14	0.07
BMI at OGTT	−0.01	0.87	−0.21	0.01	−0.20	0.01	−0.15	0.06	−0.16	0.04
GWG	−0.11	0.15	0.14	0.07	0.06	0.44	0.13	0.08	0.07	0.37
TG	0.04	0.59	−0.05	0.45	−0.02	0.83	−0.06	0.42	−0.10	0.17
CHOL	0.05	0.50	0.10	0.16	0.07	0.31	0.08	0.23	0.10	0.17
HDL	0.07	0.31	0.02	0.77	0.10	0.15	0.10	0.16	0.15	0.04
LDL	0.03	0.71	0.07	0.30	0.06	0.42	0.05	0.49	0.05	0.44
FPG	0.18	0.01	−0.07	0.35	−0.09	0.22	−0.14	0.05	−0.10	0.15
1h-PG	0.13	0.07	−0.19	0.01	−0.23	<0.01	−0.25	<0.01	−0.26	<0.01
2h-PG	0.08	0.27	−0.21	<0.01	−0.27	<0.01	−0.31	<0.01	−0.28	<0.01
HbA_{1c}	0.12	0.09	−0.24	<0.01	−0.18	0.01	−0.22	<0.01	−0.25	<0.01
Birth weight	−0.14	0.07	0.05	0.48	−0.03	0.69	0.08	0.29	0.06	0.39

Correlation between exosomal miRNAs (comparative cycle threshold method) and clinical indicators in all samples. Spearman correlation (*r*) was applied to analyze the correlation data. $P < 0.05$ was considered significant. CHOL, cholesterol; TG, triglyceride.

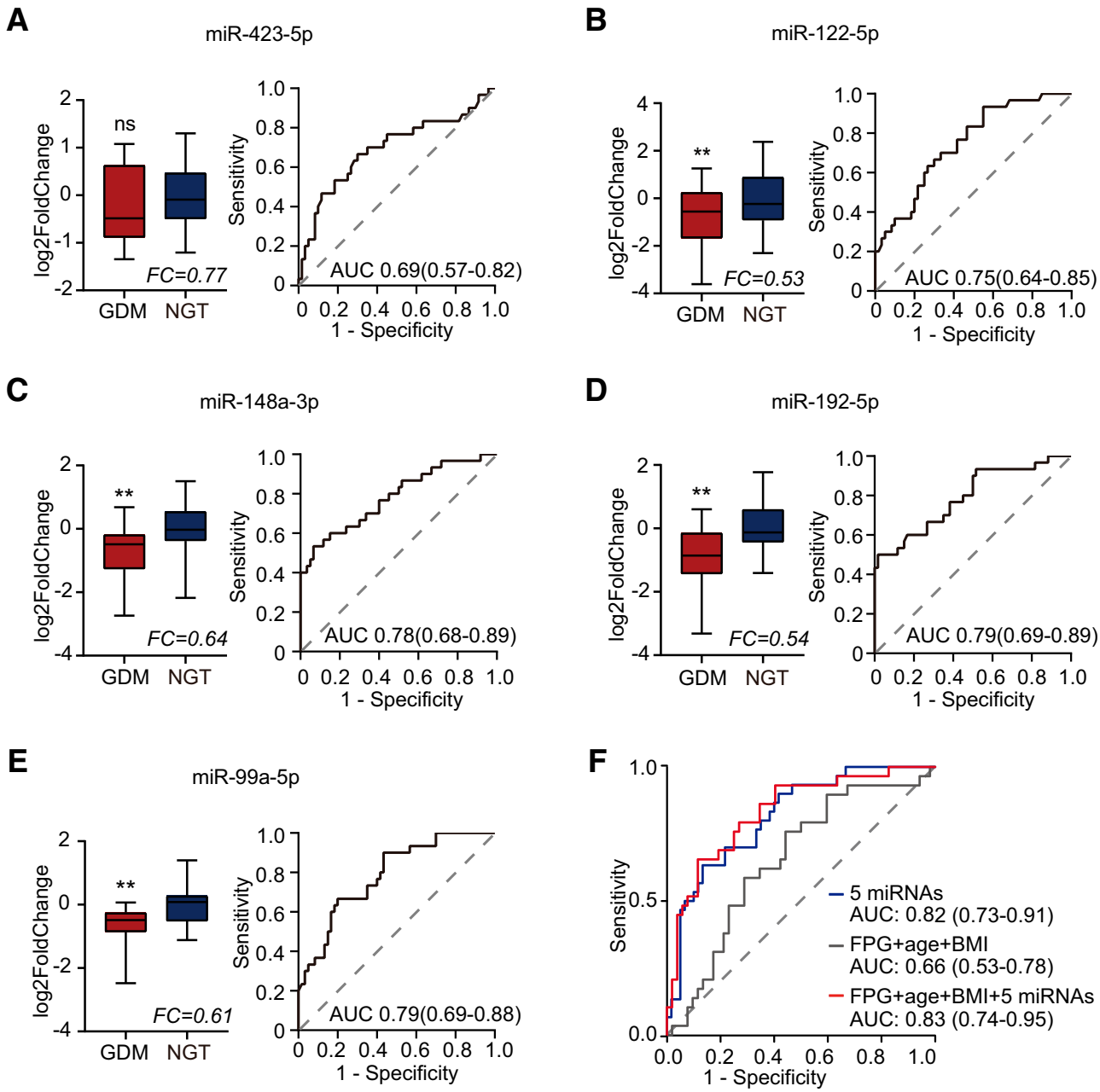

Figure 3— Early prediction of GDM by plasma exosomal miRNAs. (*A–E*) Expression of exosomal miR-423-5p (*A*, left), miR-122-5p (*B*, left), miR-148a-3p (*C*, left), miR-192-5p (*D*, left), and miR-99a-5p (*E*, left) at 10–16 gws and early predictive power of these five miRNAs for GDM (*A–E*, right) (n = 30 in GDM group; n = 60 in NGT group). (*F*) The area AUC of the five miRNAs combined for early prediction of GDM was superior to the combination of FPG at 10–16 gws, maternal age, and prepregnancy BMI, and similar to the combination of all. Data are shown as log2 fold change compared with the NGT group. *$P < 0.05$, **$P < 0.01$, ***$P < 0.001$.

prepregnancy BMI (AUC 0.66; 95% CI 0.53–0.78) and was similar to the combination of base model and associated miRNAs (AUC 0.83; 95% CI 0.74–0.95) (Fig. 3*F*). In NRI analysis, adding miRNAs to the base model significantly improved the classification accuracy with an overall categorical NRI of 86% (95% CI 29–133%; $P < 0.01$), 41% (95% CI 6–70%; $P = 0.01$) for GDM, and 45% (95% CI 12–70%; $P < 0.01$) for NGT. A significantly greater improvement in the continuous NRI was also observed (Supplementary Table 4).

Pathway Analysis of miRNA Differentially Expressed in Plasma Exosomes

Kyoto Encyclopedia of Genes and Genomes (KEGG) pathway enrichment analysis was performed to investigate the potential regulated pathways of predicted targets (Table 3). The results showed that the most enriched pathways of miR-423–5p targets were linked to MAPK and GnRH signaling pathways. The targets of miR-122–5p were linked primarily to insulin signaling pathways. The targets of miR-148a-3p were related to the FoxO signaling

Table 3—KEGG analysis of the predicted target genes of miRNAs

	Identifier	Description	Gene count, *n*	*P*	Adjusted *P*
miR-423–5p	hsa04010	MAPK signaling pathway	52	0.000004	0.000969
	hsa04912	GnRH signaling pathway	23	0.000009	0.000969
	hsa05225	Hepatocellular carcinoma	34	0.000010	0.000969
	hsa04520	Adherens junction	19	0.000017	0.001256
	hsa04934	Cushing syndrome	31	0.000030	0.001825
miR-1122–5p	hsa05220	Chronic myeloid leukemia	22	0.000014	0.004384
	hsa05222	Small-cell lung cancer	24	0.000040	0.006127
	hsa05205	Proteoglycans in cancer	41	0.000088	0.00908
	hsa05225	Hepatocellular carcinoma	35	0.000136	0.009921
	hsa04910	Insulin signaling pathway	30	0.000161	0.009921
miR-148a-3p	hsa05220	Chronic myeloid leukemia	31	1.67×10^{-10}	5.18×10^{-8}
	hsa04068	FoxO signaling pathway	42	8.43×10^{-10}	8.80×10^{-8}
	hsa01522	Endocrine resistance	35	8.49×10^{-10}	8.80×10^{-8}
	hsa04218	Cellular senescence	46	6.93×10^{-9}	5.39×10^{-7}
	hsa05205	Proteoglycans in cancer	53	2.38×10^{-8}	1.48×10^{-6}
miR-192–5p	hsa04390	Hippo signaling pathway	25	0.000048	0.007746
	hsa03440	Homologous recombination	11	0.000073	0.007746
	hsa04550	Signaling pathways regulating pluripotency of stem cells	23	0.000080	0.007746
	hsa04110	Cell cycle	21	0.000104	0.007746
	hsa04218	Cellular senescence	24	0.000241	0.014406
miR-99a-5p	hsa04115	p53 signaling pathway	11	0.000001	0.000315
	hsa04218	Cellular senescence	15	0.000008	0.001061
	hsa05205	Proteoglycans in cancer	16	0.000038	0.003341
	hsa05203	Viral carcinogenesis	15	0.000117	0.007751
	hsa04933	AGE-RAGE signaling pathway in diabetic complications	10	0.000158	0.008414

KEGG pathway enrichment analysis was performed using the predicted targets of the five differentially expressed exosomal miRNAs (miR-423–5p, 1,769 targets; miR-122–5p, 2,202 targets; miR-148a-3p, 2,218 targets; miR-192–5p, 1,569 targets; and miR-99a-5p, 459 targets). The top five pathways of each miRNA are shown. AGE, advanced glycation end products; KEGG, Kyoto Encyclopedia of Genes and Genomes; RAGE, receptor for advanced glycation end products.

pathway and endocrine resistance. The targets of miR-192–5p were involved in the Hippo signaling pathway and cellular senescence. The targets of miR-99a-5p were associated with cellular senescence and the p53 signaling pathway.

Target Genes of Differentially Expressed Plasma Exosomal miRNAs

We predicted 1,769 targets of miR-423–5p, 2,202 targets of miR-122–5p, 2,218 targets of miR-148a-3p, 1,569 targets of miR-192–5p, and 459 targets of miR-99a-5p (data not shown). To further identify the targets of the five differentially expressed exosomal miRNAs, we performed transcriptome sequencing on miRNA-overexpressed HepG2 cells (Supplementary Fig. 2). After miR-423–5p overexpression, we detected 15 downregulated genes, two of which have targeted binding sites for miR-423–5p. Among the 42 genes with low expression in miR-122–5p overexpression cells, 16 have targeted binding sites for miR-122–5p. In miR-148a-3p overexpressed cells, we found 38 genes with low expression, and eight of them have targeted binding sites for miR-148a-3p. A total of 22 downregulated genes were detected after miR-99a-5p overexpression, but none of them putatively bound to miR-99a-5p (Fig. 4*A*). The mRNA profile of cells transfected with miR-192–5p was not determined, because of low transfection efficiency. Consequently, we obtained two potential target genes for miR-423–5p, 16 for miR-122–5p, and eight for miR-148a-3p. In addition, after undergoing a literature review, 35 predicted genes (Supplementary Fig. 3*C*) from the computationally predicted targets in the insulin signaling pathway (Supplementary Fig. 3*A*) and the AMPK signaling pathway (Supplementary Fig. 3*B*) were also selected for further identification.

To examine miRNA-mRNA regulation, we explored the effects of mRNA expression of target genes in HepG2 cells transfected with mimics or inhibitors of miRNAs (Supplementary Table 5). The expression of AGK, GYS1, and IGF1R mRNAs was significantly reduced after miR-423–5p overexpression and was elevated after miR-423–5p inhibition (Fig. 4*B*, left). This method also identified the inhibition of ACACB, CREB1, FDFT1, G6PC3, NPC1L1, and PHKA2 mRNAs by miR-122–5p (Fig. 4*C*, left); of HMGCS1 and PDHA1mRNAs by miR-192–5p (Fig. 4*D*, left); and of CXCL16, PCSK9, and VLDLR mRNAs by miR-99a-5p (Fig. 4*E*, left). No target gene of miR-148a-3p was confirmed in

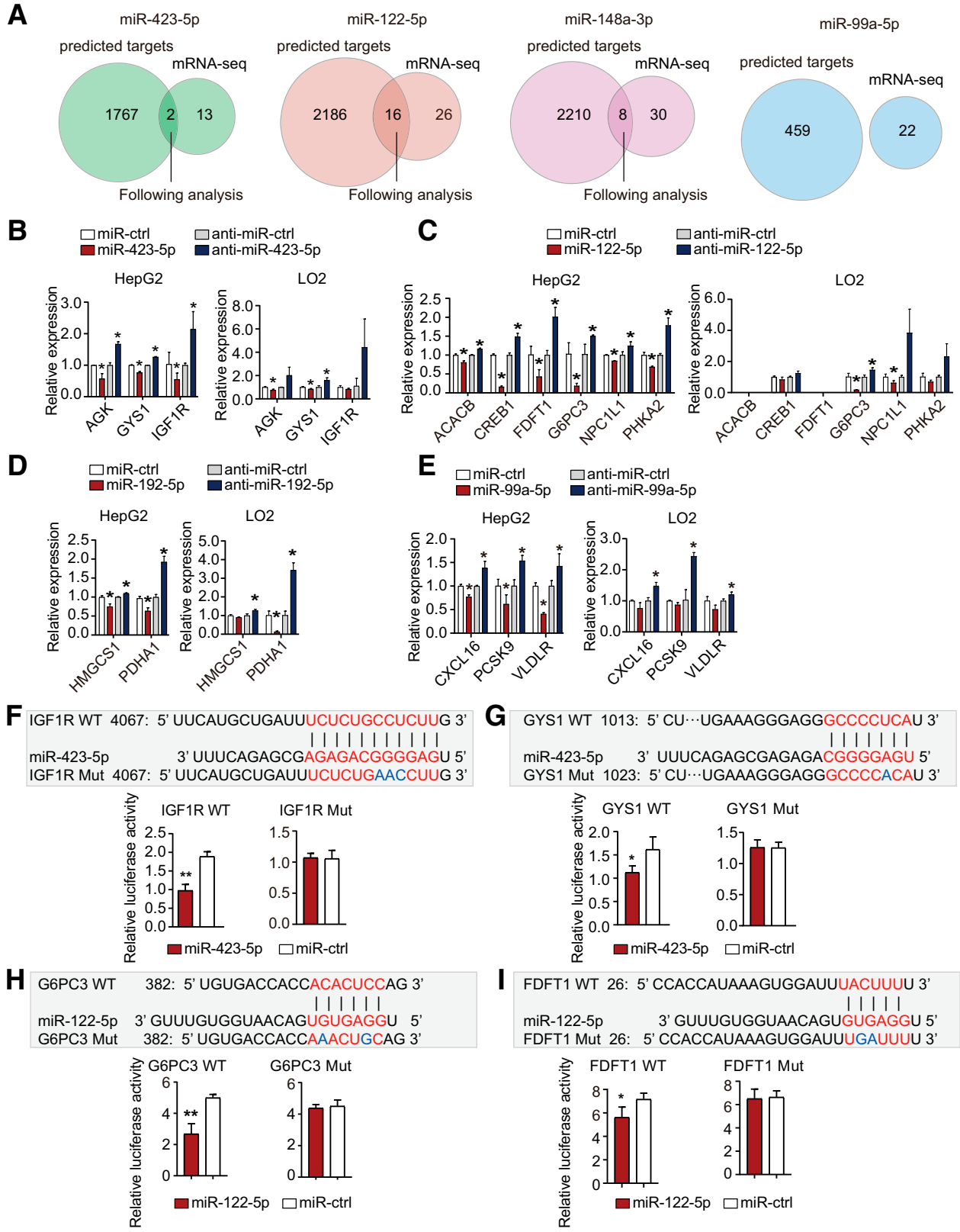

Figure 4—The expression of target genes in HepG2 cells and LO2 cells transfected with mimics or inhibitors of miRNAs. (*A*) Genes with low expression in miRNA-overexpressed HepG2 cells have targeted binding sites for miRNA. (*B–E*) Expression of target genes of miRNAs after transfection of miR-423–5p (*B*), miR-122–5p (*C*), miR-192–5p (*D*), and miR-99a-5p (*E*) in HepG2 cells (left) and LO2 cells (right). (*F–I*) Luciferase activity of HEK293 cells after cotransfection of a reporter construct containing the 3′UTR region of targets with either the

this step. Predicted targets of the miRNAs that were not identified by qRT-PCR are shown in Supplementary Fig. 4.

To confirm the targeted relationship between miRNAs and mRNA in cells from other tissues or sources, we performed real-time qPCR on LO2, skeletal muscle cells (C2C12), islet cells (MIN6), and adipocytes (3T3-L1). In LO2 cells, we confirmed the regulation of GYS1 by miR-423–5p, the regulation of G6PC3 by miR-122–5p, and the regulation of PDHA1 by miR-192–5p (Fig. 4*B–E*, right). However, we were not able to verify any targeted relationships in C2C12 cells (Supplementary Fig. 5), MIN6 cells (Supplementary Fig. 6), or 3T3-L1 cells (Supplementary Fig. 7), because most of these predicted targets were either minimally expressed or undetectable.

To further confirm whether these miRNAs directly target their downstream mRNAs, we performed luciferase reporter assays for their target mRNA 3′UTR regions correspondingly containing the predicted miRNA target sites. After overexpression of miR-423–5p, luciferase activity for IGF1R 3′UTR was diminished, whereas mutagenesis of the predicted target sites of miR-423–5p in the IGF1R 3′UTR abolished the effects of miR-423–5p overexpression on luciferase activity (Fig. 4*F*). Similarly, we confirmed that miR-423–5p directly targeted GYS1 (Fig. 4*G*) and miR-122–5p directly targeted G6PC3 (Fig. 4*H*) and FDFT1 (Fig. 4*I*).

DISCUSSION

The discovery of biomarkers associated with the underlying molecular mechanisms is of critical significance in preventing maternal–fetal complications during pregnancy. In this study, we determined the differential expression of exosomal miR-423–5p, miR-122–5p, miR-148a-3p, miR-192–5p, and miR-99a-5p between plasma from pregnant women with GDM and those with NGT. We applied the five altered miRNAs to early prediction of GDM in a nested case–control study and found that these exosomal miRNA profiles predict GDM with an AUC of 0.82 as early as 10–16 gws. We identified that miR-423–5p and miR-122–5p regulate target genes, such as IGF1R, GYS1, G6PC3, and FDFT1, involved in the metabolic signaling pathways (Supplementary Fig. 8).

Exosomes have been shown to differ between pregnancies of women with GDM and of women with NGT (25), and many attempts have been made to illustrate the specific miRNA profiling in GDM exosomes (26, 30). To our knowledge, the present study is the first confirmative research on GDM-specific, circulating, exosomal miRNA profiling based on NGS and large-scale validation. This study, to our knowledge, is the first to report the upregulation of miR-423–5p and the decreased expression of miR-122–5p, miR-148a-3p, miR-192–5p, and miR-99a-5p in GDM plasma exosomes.

To investigate whether these alterations of exosomal miRNAs are detectable in the pregnancy period earlier than 24–28 gws and to examine the predictive value of the differential miRNA profile, we performed a diagnostic test in a nested case–control study based on a prospective cohort. Our results illustrated that these circulating exosomal miRNAs improved the early prediction of GDM, together with classical risk factors. The predictive power of our study outperforms previous predictions using lipid biomarkers (31), random plasma glucose (32), or serum metabolites (33).

The differentially expressed miRNAs we found in this study were associated with the underlying mechanism of insulin resistance and hyperglycemia. The finding that exosomal miR-423–5p was elevated in GDM is consistent with previous reports on upregulation of miR-423–5p in obesity (34) and type 2 diabetes mellitus (35). We identified IGF1R and GYS1 as targets of miR-423–5p. IGF1R is highly homologous to the insulin receptor (36), and inhibition of IGF1R may impair the insulin signaling pathway (37). Downregulation of GYS1 leads to low expression of glycogen synthase, which affects glucose homeostasis (38).

The downregulation of miR-122–5p in GDM plasma exosomes was also related to the modulation of glucose metabolism. A previous study found that a decrease of miR-122 leads to hepatic insulin resistance (39). In gestationally obese women, miR-122 was negatively correlated with HOMA of insulin resistance, C-peptide, and triglyceride values (40). A decrease of miR-122–5p may affect glucose metabolism by G6PC3 (41). Glucose 6 phosphatase is a key enzyme in gluconeogenesis; G6PC3 expression in glycogen trophoblast cells is associated with glucose production (42). FDFT1, the other target of miR-122–5p, is increased in obesity-related type 2 diabetes (43) and can inhibit glycolysis and reduce glucose uptake through suppression of the AKT-mTOR-HIF1α pathway (44).

Our finding that low expression of exosomal miR-148a-3p and miR-192–5p in the plasma of the GDM group coincides with results of a previous study showing the downregulation of miR-148a-3p and miR-192–5p in exosomes derived from the chorionic villous cells of the placenta from pregnancies involving GDM (30). Moreover, miR-148a-3p and miR-192–5p were reported to be involved in metabolic regulation in several other studies, which are summarized in Supplementary Table 6 (45–50). Therefore, more studies using placenta-derived exosomes are needed to determine whether the placenta contributes to low expression of exosomal miR-148a-3p and miR-192–

miRNA mimic control or miRNA mimic. (*F*) miR-423–5p directly targets IGF1R. (*G*) miR-423–5p directly targets GYS1. (*H*) miR-122–5p directly targets G6PC3. (*I*) miR-122–5p directly targets FDFT1. The binding site of miRNAs on their target was predicted by TargetScan 7.2. mut, mutant; WT, wild type. $*P < 0.05$, $**P < 0.01$.

5p in circulation of women whose pregnancy is complicated by GDM.

This study has several strengths. First, we performed small-RNA NGS to identify exosomal miRNA profiles in GDM and used a larger number of clinical samples to increase the certainty of differentially expressed miRNAs. Second, we developed a prediction strategy using exosomal miRNA profiling for GDM through a nested case–control study based on a prospective cohort between 10 and 16 gws. Third, we identified several miRNA–mRNA regulatory networks using compounding experiments. Therefore, our research not only confirms that miRNAs related to glucose metabolism have an early predictive value but also provides information for additional research about the pathogenesis of GDM.

This study has some limitations. First, the source of the exosomes in plasma was not identified. Second, the exosomal miRNA profile in late gestation was not obtained, and the longitudinal variation of miRNA expression remains unclear. Third, involvement of predicted target genes from multiple prediction websites increased the false-positive rate of target verification. Another limitation is that identification of miRNA targets by mRNA expression may miss some miRNA–mRNA pairs with imperfect complementarity binding, which may block the mRNA translation without degradation.

In conclusion, we developed an early screening strategy for GDM by plasma exosomal miRNAs based on their underlying biological functions. The efficiency of this predicted method requires further evaluation in a large-scale prospective-cohort study.

Acknowledgments. The authors thank Prof. Jianrong Yang in the Department of Biology, Zhongshan School of Medicine, Sun Yat-sen University, for providing analysis platform for Next Generation Sequencing data. We are grateful to Prof. Shawn Li from Western University and Prof. Phei Er Saw from Sun Yat-sen Memorial Hospital of Sun Yat-sen University for reviewing the manuscript. We also thank Alyssa Wu of Western University for editing the manuscript.

Funding. This work was supported by the National Natural Science Foundation of China (grants 81771602 and 81300493 to B.L. and 81701378 to Z.W.); Natural Science Foundation of Guangdong Province (grants 2017A030313826 to B.L. and 2017A020214014 to Z.W.); Sun Yat-Sen University Clinical Research 5010 Program (grants 2016014 to B.L. and 201204 to Z.W.); Fundamental Research Funds for the Central Universities (grant 16ykpy19 to B.L.); and National Key Research and Development Program of China (grant 2021YFC2700700, subgrant to Z.W.).

The funders had no role in study design, data collection and analysis, decision to publish, or preparation of the manuscript.

Duality of Interest. No potential conflicts of interest relevant to this article were reported.

Author Contributions. B.L. and Z.Y. designed the study, analyzed data, and drafted the manuscript. S.W., S. Li., and P.C. input participants data, collected clinical data, and prepared samples. Z.Y., X.H., and S. Lin performed bioinformatics analysis, qRT-PCR, Western blotting, luciferase reporter assay, and other related experiments. L.D. provided laboratory data. Z.W. critically reviewed the manuscript. B.L. is the guarantor of this work and, as such, had full access to all the data in the study and takes responsibility for the integrity of the data and the accuracy of the data analysis.

References

1. Feghali MN, Scifres CM. Novel therapies for diabetes mellitus in pregnancy. BMJ 2018;362:k2034

2. McIntyre HD, Catalano P, Zhang C, Desoye G, Mathiesen ER, Damm P. Gestational diabetes mellitus. Nat Rev Dis Primers 2019;5:47

3. American Diabetes Association. 2. Classification and diagnosis of diabetes: *Standards of Medical Care in Diabetes-2020*. Diabetes Care 2020;43(Suppl. 1):S14–S31

4. Liu B, Cai J, Xu Y, et al. Early diagnosed gestational diabetes mellitus is associated with adverse pregnancy outcomes: a prospective cohort study. J Clin Endocrinol Metab 2020;105:dgaa633

5. Saravanan P; Diabetes in Pregnancy Working Group; Maternal Medicine Clinical Study Group; Royal College of Obstetricians and Gynaecologists, UK. Gestational diabetes: opportunities for improving maternal and child health. Lancet Diabetes Endocrinol 2020;8:793–800

6. Metzger BE, Gabbe SG, Persson B, et al.; International Association of Diabetes and Pregnancy Study Groups Consensus Panel. International Association of Diabetes and Pregnancy study groups recommendations on the diagnosis and classification of hyperglycemia in pregnancy. Diabetes Care 2010;33:676–682

7. World Health Organization. *Diagnostic Criteria and Classification of Hyperglycaemia First Detected in Pregnancy.* Geneva, Switzerland, World Health Organization, 2013.

8. Sweeting AN, Ross GP, Hyett J, Wong J. Gestational diabetes in the first trimester: is early testing justified? Lancet Diabetes Endocrinol 2017;5:571–573

9. Tu WJ, Guo M, Shi XD, Cai Y, Liu Q, Fu CW. First-trimester serum fatty acid-binding protein 4 and subsequent gestational diabetes mellitus. Obstet Gynecol 2017;130:1011–1016

10. Wnuk A, Stangret A, Wątroba M, et al. Can adipokine visfatin be a novel marker of pregnancy-related disorders in women with obesity? Obes Rev 2020;21:e13022

11. Zhong L, Long Y, Wang S, et al. Continuous elevation of plasma asprosin in pregnant women complicated with gestational diabetes mellitus: a nested case-control study. Placenta 2020;93:17–22

12. Huang Y, Chen X, Chen X, et al. Angiopoietin-like protein 8 in early pregnancy improves the prediction of gestational diabetes. Diabetologia 2018;61:574–580

13. Koos BJ, Gornbein JA. Early pregnancy metabolites predict gestational diabetes mellitus: implications for fetal programming. Am J Obstet Gynecol. 2021;224:215.e1-.e7.

14. Mihaylova MM, Shaw RJ. The AMPK signalling pathway coordinates cell growth, autophagy and metabolism. Nat Cell Biol 2011;13:1016–1023

15. Hoshino A, Kim HS, Bojmar L, et al. Extracellular vesicle and particle biomarkers define multiple human cancers. Cell 2020;182:1044–1061.e18

16. Mori MA, Ludwig RG, Garcia-Martin R, Brandão BB, Kahn CR. Extracellular miRNAs: from biomarkers to mediators of physiology and disease. Cell Metab 2019;30:656–673

17. Hosseini R, Sarvnaz H, Arabpour M, et al. Cancer exosomes and natural killer cells dysfunction: biological roles, clinical significance and implications for immunotherapy. Mol Cancer 2022;21:15

18. Arbo BD, Cechinel LR, Palazzo RP, Siqueira IR. Endosomal dysfunction impacts extracellular vesicle release: central role in Aβ pathology. Ageing Res Rev 2020;58:101006

19. Kahn CR, Wang G, Lee KY. Altered adipose tissue and adipocyte function in the pathogenesis of metabolic syndrome. J Clin Invest 2019;129:3990–4000

20. Ying W, Gao H, Dos Reis FCG, et al. MiR-690, an exosomal-derived miRNA from M2-polarized macrophages, improves insulin sensitivity in obese mice. Cell Metab 2021;33:781–790.e5

21. Li J, Zhang Y, Ye Y, et al. Pancreatic β cells control glucose homeostasis via the secretion of exosomal miR-29 family. J Extracell Vesicles 2021;10:e12055

22. Castaño C, Mirasierra M, Vallejo M, Novials A, Párrizas M. Delivery of muscle-derived exosomal miRNAs induced by HIIT improves insulin sensitivity through down-regulation of hepatic FoxO1 in mice. Proc Natl Acad Sci USA 2020;117:30335–30343
23. Sheller-Miller S, Radnaa E, Yoo JK, et al. Exosomal delivery of NF-κB inhibitor delays LPS-induced preterm birth and modulates fetal immune cell profile in mouse models. Sci Adv 2021;7:eabd3865
24. Ayala-Ramírez P, Machuca-Acevedo C, Gámez T, et al. Assessment of placental extracellular vesicles-associated Fas ligand and TNF-related apoptosis-inducing ligand in pregnancies complicated by early and late onset preeclampsia. Front Physiol 2021;12:708824
25. Salomon C, Scholz-Romero K, Sarker S, et al. Gestational diabetes mellitus is associated with changes in the concentration and bioactivity of placenta-derived exosomes in maternal circulation across gestation. Diabetes 2016;65:598–609
26. Gillet V, Ouellet A, Stepanov Y, et al. miRNA profiles in extracellular vesicles from serum early in pregnancies complicated by gestational diabetes mellitus. J Clin Endocrinol Metab 2019;104:5157–5169
27. Kandzija N, Zhang W, Motta-Mejia C, et al. Placental extracellular vesicles express active dipeptidyl peptidase IV; levels are increased in gestational diabetes mellitus. J Extracell Vesicles 2019;8:1617000
28. Gupta Y, Kalra B, Baruah MP, Singla R, Kalra S. Updated guidelines on screening for gestational diabetes. Int J Womens Health 2015;7:539–550
29. Agarwal V, Bell GW, Nam JW, Bartel DP. Predicting effective microRNA target sites in mammalian mRNAs. eLife 2015;4:e05005
30. Nair S, Jayabalan N, Guanzon D, et al. Human placental exosomes in gestational diabetes mellitus carry a specific set of miRNAs associated with skeletal muscle insulin sensitivity. Clin Sci (Lond) 2018;132:2451–2467
31. Lu L, Koulman A, Petry CJ, et al. An unbiased lipidomics approach identifies early second trimester lipids predictive of maternal glycemic traits and gestational diabetes mellitus. Diabetes Care 2016;39:2232–2239
32. Meek CL, Murphy HR, Simmons D. Random plasma glucose in early pregnancy is a better predictor of gestational diabetes diagnosis than maternal obesity. Diabetologia 2016;59:445–452
33. Enquobahrie DA, Denis M, Tadesse MG, Gelaye B, Ressom HW, Williams MA. Maternal early pregnancy serum metabolites and risk of gestational diabetes mellitus. J Clin Endocrinol Metab 2015;100:4348–4356
34. Prats-Puig A, Ortega FJ, Mercader JM, et al. Changes in circulating microRNAs are associated with childhood obesity. J Clin Endocrinol Metab 2013;98:E1655–E1660
35. Prabu P, Rome S, Sathishkumar C, et al. Circulating miRNAs of 'Asian Indian phenotype' identified in subjects with impaired glucose tolerance and patients with type 2 diabetes. PLoS One 2015;10:e0128372
36. Siddle K. Signalling by insulin and IGF receptors: supporting acts and new players. J Mol Endocrinol 2011;47:R1–R10
37. Ansarullah JC, Far FF, Homberg S, et al. Inceptor counteracts insulin signalling in β-cells to control glycaemia. Nature 2021;590:326–331
38. Xirouchaki CE, Mangiafico SP, Bate K, et al. Impaired glucose metabolism and exercise capacity with muscle-specific glycogen synthase 1 (gys1) deletion in adult mice. Mol Metab 2016;5:221–232
39. Yang YM, Seo SY, Kim TH, Kim SG. Decrease of microRNA-122 causes hepatic insulin resistance by inducing protein tyrosine phosphatase 1B, which is reversed by licorice flavonoid. Hepatology 2012;56:2209–2220
40. Carreras-Badosa G, Bonmatí A, Ortega FJ, et al. Altered circulating miRNA expression profile in pregestational and gestational obesity. J Clin Endocrinol Metab 2015;100:E1446–E1456
41. Tsai WC, Hsu PW, Lai TC, et al. microRNA-122, a tumor suppressor microRNA that regulates intrahepatic metastasis of hepatocellular carcinoma. Hepatology 2009;49:1571–1582
42. Roberts GAG, Tunster SJ. Characterising the dynamics of placental glycogen stores in the mouse. Placenta 2020;99:131–140
43. Ding J, Reynolds LM, Zeller T, et al. Alterations of a cellular cholesterol metabolism network are a molecular feature of obesity-related type 2 diabetes and cardiovascular disease. Diabetes 2015;64:3464–3474
44. Weng ML, Chen WK, Chen XY, et al. Fasting inhibits aerobic glycolysis and proliferation in colorectal cancer via the Fdft1-mediated AKT/mTOR/HIF1α pathway suppression. Nat Commun 2020;11:1869
45. Shah KB, Chernausek SD, Teague AM, Bard DE, Tryggestad JB. Maternal diabetes alters microRNA expression in fetal exosomes, human umbilical vein endothelial cells and placenta. Pediatr Res 2021;89:1157–1163
46. Mononen N, Lyytikäinen LP, Seppälä I, et al. Whole blood microRNA levels associate with glycemic status and correlate with target mRNAs in pathways important to type 2 diabetes. Sci Rep 2019;9:8887
47. Wang J, Yao Y, Wang K, Li J, Chu T, Shen H. MicroRNA-148a-3p alleviates high glucose-induced diabetic retinopathy by targeting TGFB2 and FGF2. Acta Diabetol 2020;57:1435–1443
48. Liu XL, Cao HX, Wang BC, et al. miR-192-5p regulates lipid synthesis in non-alcoholic fatty liver disease through SCD-1. World J Gastroenterol 2017; 23:8140–8151
49. Cai H, Jiang Z, Yang X, Lin J, Cai Q, Li X. Circular RNA HIPK3 contributes to hyperglycemia and insulin homeostasis by sponging miR-192-5p and upregulating transcription factor forkhead box O1. Endocr J 2020;67:397–408
50. Li P, Fan C, Cai Y, et al. Transplantation of brown adipose tissue up-regulates miR-99a to ameliorate liver metabolic disorders in diabetic mice by targeting NOX4. Adipocyte 2020;9:57–67